

Contact-Induced Transverse Fractures in Brittle Layers on Soft Substrates: A Study on Silicon Nitride Bilayers

Kee Sung Lee,[†] Sataporn Wuttiphon,[‡] Xiao-Zhi Hu,[§] Seung Kun Lee,^{*,||} and Brian R. Lawn^{*}

Materials Science and Engineering Laboratory, National Institute of Standards and Technology, Gaithersburg, Maryland 20899

An analysis of transverse cracks induced in brittle coatings on soft substrates by spherical indenters is developed. The transverse cracks are essentially axisymmetric and geometrically conelike, with variant forms dependent on the location of initiation: outer cracks that initiate at the top surface outside the contact and propagate downward; inner cracks that initiate at the coating/substrate interface beneath the contact and propagate upward; intermediate cracks that initiate within the coating and propagate in both directions. Bilayers consisting of hard silicon nitride (coating) on a composite underlayer of silicon nitride with boron nitride platelets (substrate), with strong interfacial bonding to minimize delamination, are used as a model test system for Hertzian testing. Test variables investigated are contact load, coating/substrate elastic-plastic mismatch (controlled by substrate boron nitride content), and coating thickness. Initiation of the transverse coating cracks occurs at lower critical loads, and shifts from the surface to the interface, with increasing elastic-plastic mismatch and decreasing coating thickness. This shift is accompanied by increasing quasi-plasticity in the substrate. Once initiated, the cracks pop in and arrest within the coating, becoming highly stabilized and insensitive to further increases in contact load, or even to coating toughness. A finite element analysis of the stress fields in the loaded layer systems enables a direct correlation between the damage patterns and the stress distributions: between the transverse cracks and the tensile (and compressive) stresses; and between the subsurface yield zones and the shear stresses. Implications of these conclusions concerning the design of coating systems for damage tolerance are discussed.

I. Introduction

THE mechanics of contact-induced cracks in hard, brittle layers on deformable but tough substrates are of interest in relation to the potential failure of practical coating systems in concentrated loadings. Examples include wear-resistant ceramic coatings on metal substrates,^{1,2} thermal barrier coatings,^{3,4} ceramic layer structures with alternating homogeneous

and heterogeneous microstructures,⁵⁻⁷ and biocoatings like teeth (enamel on dentin) and bone. The chief aim in designing such systems is to provide an optimum combination of underlying substrate toughness with surface protection by the coating layer. In terms of failure mode, the literature has focused almost exclusively on delamination at the coating/substrate interfaces;⁸⁻¹⁰ indeed, existing engineering design virtually mandates that these interfaces be made weak, in order to deflect cracks and so enhance the toughness.¹¹ More recently, however, layer structures have been fabricated with relatively strong interfaces, with the explicit aim of suppressing the delamination failure mode and relying on the substrate to absorb penetrant fractures.^{5,6,12,13} The limiting factor then becomes the brittle failure of the coating itself.

The layer fractures under explicit consideration here are those of near-axisymmetric form that initiate from the top surface at external contacts and that propagate transversely through the coating. These transverse cracks are most readily studied using spherical indenters ("Hertzian contact").^{5,6} They are of practical importance because they provide for potential removal of part or all of the coating and for access of the environment to the substrate. Two forms of these fractures have been previously identified:^{5,6} cracks that initiate at the coating-free surface outside the contact circle and extend downward; cracks that initiate at the coating/substrate interface within the contact circle and extend upward. We shall encounter both forms here, plus another that initiates between the first two from within the coating interior. We propose that all such transverse cracks can be usefully considered in terms of a generic quasi-conical geometry.

The principal aim of this paper is to demonstrate the fundamental nature of this class of contact-induced transverse cracks, and to describe the stress states that drive them. As a model material system for study we choose a composite silicon nitride bilayer system with large elastic-plastic mismatch.^{7,14} The top coating layer is a hard, wear-resistant silicon nitride of moderate grain size; the underlying substrate layer is a relatively soft, damage-tolerant silicon nitride material with boron nitride platelet inclusions. Hertzian contacts are used to induce the damage in the layered specimens, and ceramographic sectioning techniques are used to examine these damage patterns. Key variables investigated are coating layer thickness, ranging from 120 to 1200 μm , and substrate composition, ranging from 5 to 30 wt% boron nitride additive phase. We show that crack densities in the coating increase with decreasing coating thickness and with increasing substrate boron nitride content. Quasi-plastic deformation^{††} in the soft underlayer (and to a lesser extent also in the coating) enhances the cracking. Once initiated, the cracks are highly stable, somewhat insensitive in dimension to the contact load and to material (and environment) properties such as toughness, arresting as they approach the bounding surfaces or interfaces of the coating. This arrest con-

J. E. Ritter—contributing editor

Manuscript No. 191250. Received January 24, 1997; approved June 19, 1997.

Supported by the U.S. Air Force Office of Scientific Research. Additional support for K. S. Lee was provided by the Korea Advanced Institute of Science and Technology (KAIST) Ph.D. program. S. Wuttiphon received financial support from the Royal Thai Scholarship program.

[†]Member, American Ceramic Society.

[‡]Graduate Student at the Department of Materials Science and Engineering, Korea Advanced Institute of Science and Technology, Yusong, Taejeon 305-701, Korea.

[§]Graduate Student at the Department of Materials and Nuclear Engineering, University of Maryland, College Park, Maryland 20742.

^{||}Guest Scientist from the Department of Mechanical and Materials Engineering, University of Western Australia, Nedlands, WA 6907, Australia.

^{*}Guest Scientist from the Department of Materials Science and Engineering, Lehigh University, Pennsylvania 18015.

^{††}We use the term "quasi-plasticity" in the context of ceramics that deform by a microstructural shear fault mode,¹⁵ to distinguish from traditional dislocation-driven plasticity deformation in metals.

dition leads to multiple but still-confined cracking at higher loads, plus some subsidiary cracking in the substrate, contributing to the damage tolerance of these structures. Ultimately, at even higher loads, the coating fails.

Stress analysis of the Hertzian-type contact fields in the coating/substrate structures is conducted using finite element modeling (FEM). Attention is focused on the distributions of principal tensile stresses, to quantify the fracture patterns, and shear stresses, to quantify the quasi-plastic zones. These considerations confirm that the cracks propagate in predominantly mode I, and highlight the role of elastic-plastic mismatch in enhancing these fractures. Calculations performed for the different experimental coating thicknesses and substrate compositions show how the tensile stress distributions are modified by layer geometry and degree of mismatch. In particular, these calculations reveal how the nature of the stress field changes from essentially classical Hertzian, in thick coatings with low substrate mismatch, to essentially flexural, in thin coatings with high substrate mismatch.

II. Experiment and Calculation

(1) Processing and Preparation of Silicon Nitride Bilayer Specimens

Silicon nitride bilayers were prepared using a derivative of the procedures previously described for producing monolithic¹⁶ and multilayer structures.^{7,14} A common powder processing and firing procedure was used for the coating and substrate layers, to ensure strong interlayer bonding in the finished product.

The silicon nitride starting powder for the coating layers was α -Si₃N₄ (UBE-SN-E10, Ube Industries, Tokyo, Japan) with sintering additives 2 wt% Al₂O₃ (AKP50, Sumitomo Chemical Co. Ltd., Tokyo, Japan), 5 wt% Y₂O₃ (H. C. Starck GmbH, Goslar, Germany), and 1 wt% MgO (High Purity, Baikowski Co., NC). Substrate layer compositions were prepared from the same starting powder, but with BN (Aldrich Chemical, Milwaukee, WI) additions of 5, 10, 20, 30 wt%. All powder batches were ball-milled using alumina balls in isopropyl alcohol for 24 h. After oven drying and sieving, the powder mixes were cold-pressed in a graphite mold of 50 mm diameter to form green state bilayers of coating thickness 1–2 mm and substrate thickness 3–4 mm. These were then hot-pressed at 1730°C at a pressure of 30 MPa in nitrogen for 1 h.

The top surfaces of the fired bilayer specimens were then ground and polished to 1 μ m diamond paste finish to produce final coating thicknesses $d = 120, 250, 400$ and 1250μ m for indentation testing. Some side surfaces normal to the coating surface were also polished, for exploratory cross-section indentation tests. Other specimens were cut in half and the opposing surfaces polished and glued together to produce ‘‘bonded-interface’’ specimens,^{17,18} for investigation of subsurface damage in Hertzian contact tests. Microstructural examination was carried out by scanning electron microscopy (SEM).

(2) Indentation Tests

Exploratory Vickers and Hertz indentation tests were made on polished surfaces, both normal and parallel to the hot-pressing direction. One set of Vickers indentations was made at load $P = 100$ N in specimens of each of the component materials, to determine elemental deformation and fracture responses. Another set was made in polished side sections of bilayer specimens (i.e., in a plane containing the hot press direction), with the pyramid center located a fixed distance 75 μ m from the interfaces and with the diagonals aligned parallel and orthogonal to the coating/substrate interfaces, to confirm that the lower radial crack may penetrate into the substrate without substantial delamination.⁶ Hertzian indentations were made with a WC sphere of radius 1.98 mm at loads $P = 1000$ – 2000 N, symmetrically across the interfaces, as a further test for delamination.

Indentation stress-strain curves were measured on the top

surfaces of individual coating and substrate and composite bilayer specimens, using WC spherical indenters of radii $r = 1.21$ – 12.7 mm at loads up to $P = 4000$ N. For these tests, it was useful to coat the top surfaces with a gold film *before* indentation, to render the ensuing residual contact impressions visible in Nomarski illumination. From measurements of contact radius a at each value of P and r , indentation stress, $p_0 = P/\pi a^2$, and indentation strain, a/r , could be evaluated, enabling construction of the stress-strain curves. Indentations were also made on individual component materials to determine critical loads P_Y for first residual impressions, and thence yield stresses Y , from $p_Y = P_Y/\pi a^2 = 1.1Y$.¹⁹

To evaluate the contact damage, Hertzian indentations were made on polished surfaces, which were then gold coated and viewed in Nomarski contrast. Subsurface damage was examined using bonded-interface specimens. The indentations were made symmetrically along the traces of these interfaces on the top surfaces, using WC spheres of radius $r = 1.98$ mm at loads up to $P = 4000$ N. After separating the indented specimen halves in solvent, a gold coat was once more applied to the side surfaces for viewing in Nomarski contrast.

Some serial sectioning by polishing away the top indented surface was also conducted on indented bilayer specimens to confirm the crack geometry inferred from the bonded-interface specimens.

(3) FEM Analysis

An FEM algorithm, described in detail elsewhere^{20–22} and foreshadowed in earlier studies by others,^{23,24} was used to determine the contact stress fields in the bilayer systems. In this algorithm, a sphere of radius 1.98 mm is loaded incrementally onto the top surface of the prescribed layer structure. The interface between coating and substrate is maintained intact throughout the loading process. The sphere and specimen are represented by a grid with maximum mesh dimension \ll sphere radius r or coating thickness d .^{21,22}

For a given set of input parameters representing the individual bilayer materials, a stress-strain curve can be reconstructed and calibrated against corresponding experimental data (with data for the sphere material from a previous study²⁰). Input material parameters for each of the constituent layer components were determined in this way, in accordance with a shear stress criterion for deformation. This criterion is expressible in terms of a constitutive uniaxial compression stress-strain function $\sigma(\epsilon)$:^{20,21}

$$\sigma = E\epsilon \quad (\sigma \leq Y) \quad (1a)$$

$$\sigma = Y + \alpha(\epsilon E - Y) \quad (\sigma \geq Y) \quad (1b)$$

with E Young’s modulus, Y a uniaxial yield stress, and α a strain-hardening coefficient in the range $0 \leq \alpha \leq 1$ ($\alpha = 1$, elastic; $\alpha = 0$, plastic).

Calculations using this algorithm were performed for layer structures with coating thicknesses $d = 120, 250, 400,$ and 1250μ m, for each substrate composition specified in the preceding subsection. Corresponding point-by-point computations of the principal stresses $\sigma_1, \sigma_2,$ and σ_3 below the contact were derived from these calculations:^{21,22} for evaluation of fracture, contours of the most tensile stress σ_1 , and corresponding σ_2 – σ_3 stress trajectories; for evaluation of quasi-plasticity, contours of maximum principal shear stress $\tau = \frac{1}{2}(\sigma_3 - \sigma_1)$, specifically the yield zone boundary, $\tau = \frac{1}{2}Y$.

III. Results: Characterization of Layer Materials

In this section we present results of initial characterization tests carried out on the composite silicon nitride bilayer systems, beginning with the individual material components in order to establish a proper basis for the ensuing fracture analysis in Section IV. Table I summarizes the quantitative results.

(1) Basic Properties of Component Materials

SEM examinations of the polished specimens revealed microstructures similar to those reported in earlier studies, rela-

Table I. Characteristics of Coating and Substrate Materials

Composition	Hardness H (GPa) [†]	Young's modulus E (GPa)	Yield stress Y (GPa)	Strain-hardening coeff α
Si_3N_4	14.6	320	8.4	0.7
$\text{Si}_3\text{N}_4 + 5\text{BN}$	12.0	278	6.7	0.5
$\text{Si}_3\text{N}_4 + 10\text{BN}$	11.1	222	4.5	0.4
$\text{Si}_3\text{N}_4 + 20\text{BN}$	7.4	160	2.8	0.1
$\text{Si}_3\text{N}_4 + 30\text{BN}$	4.7	119	1.6	0

[†]Hardness defined as $H = P/2a^2$.

tively isotropic in the monolithic Si_3N_4 and highly anisotropic in the Si_3N_4 -BN composites. For the Si_3N_4 coating, the microstructure had elongated β grains of length $\approx 5 \mu\text{m}$ and diameter $\approx 0.8 \mu\text{m}$, with $\approx 10 \text{ wt}\%$ glassy phase.¹⁶ For the Si_3N_4 -BN substrate layer, the BN had the form of platelets $1.5\text{--}10 \mu\text{m}$ in diameter and $0.2\text{--}0.6 \mu\text{m}$ thick, with these platelets strongly aligned normal to the hot-pressing direction, i.e., parallel to the coating/substrate interfaces.⁷

Exploratory Vickers indentations on polished surfaces normal and parallel to the hot-pressing direction provided a useful semiquantitative guide to material properties. Hardness values H on bulk material surfaces were found to be insensitive to the surface orientation relative to the hot-press direction. These values are seen in Table I to decrease with increasing BN content, by more than a factor of 3 in the 30 wt% composite material, confirming the softening effect of the additive phase. No such isotropy was apparent in the radial crack patterns. In the substrate materials the radial crack lengths were markedly greater in the direction normal to the hot-pressing direction, by $\approx 40\%$ in Si_3N_4 -10% BN, $\approx 80\%$ in Si_3N_4 -20% BN, and $\approx 120\%$ in Si_3N_4 -30% BN. This trend is consistent with the observed textural anisotropy in the composite structures. (A smaller discrepancy of $<10\%$, and of the same sign, was also observed in the base Si_3N_4 coating material, suggesting some minor texturing in the microstructure.) In all materials the radial cracks deflected locally along interphase boundaries, especially at the large BN platelets in the composite structures, indicating the existence of weak internal interfaces.

Values of Young's modulus E in Table I were determined for the different material components from the initially linear slopes of indentation stress-strain curves³ (see Section III(3)). The values of E decrease with increasing BN content, commensurate with a more compliant platelet phase.¹⁴ Yield stresses Y measured from first detection of residual impressions also decrease significantly with increasing BN content, in ac-

cordance with the trend in hardness values listed in Table I. These results confirm that the addition of the BN phase has a substantial softening effect on the silicon nitride structure.

(2) Crack Behavior at Coating/Substrate Interface

Vickers indentations made at polished sections of coating/substrate bilayers are useful in confirming the intrinsic strength of the interfaces. First, indentations made in the coatings and substrates away from the interfaces show the same radial crack dimensions as the tests on the bulk specimens, within experimental scatter ($\approx 5\%$). This indicates that the level of residual stress in the coating is negligibly small. Indentations made in the coating close to the interface, at fixed distance $75 \mu\text{m}$ and load $P = 100 \text{ N}$, show significant departures from symmetry. Examples are shown in Fig. 1, for substrates with 10, 20, and 30 wt% BN additive. The key observation is the absence of any delamination along the interfaces, indicating that the toughness of the interface is at least one half that of the substrate material.²⁵ Instead, the lower radial cracks penetrate into the tougher substrate (Table I), where they are arrested. Note that the initially orthogonal radial cracks appear to be attracted toward the interface as they extend, most noticeably in the bilayer with the highest BN content, as commonly observed with indentation cracks adjacent to a low modulus layer.²⁶ Hence elastic-plastic mismatch between the coating and substrate materials is a factor in the fracture behavior.

Hertzian indentations across the coating/substrate bilayer interface serve to reinforce the above Vickers results. Figure 2 shows a damage pattern using a WC sphere of $r = 1.98 \text{ mm}$ at increasing $P = 2000 \text{ N}$ on a bilayer with 10 wt% BN substrate. Multiple ring cracks initiate on the Si_3N_4 coating side, and penetrate the interface onto the Si_3N_4 -BN substrate side, where they quickly arrest. Again, delamination is absent. There is indication of a residual depression at the contact area within the ring cracks, especially in the softer substrate material.

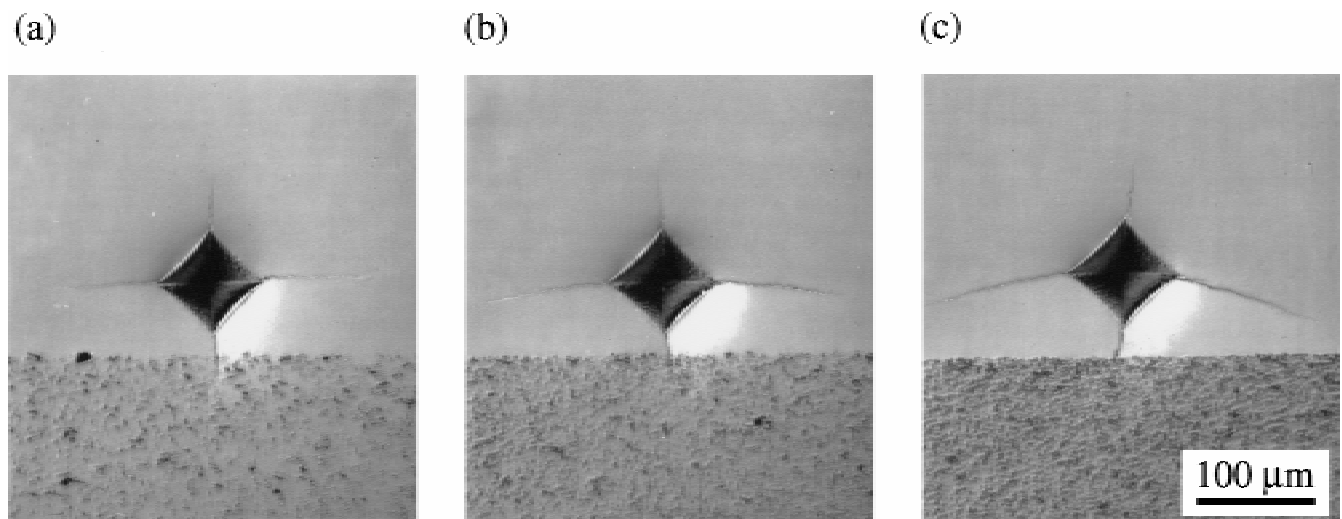


Fig. 1. Micrographs of Vickers radial cracks in Si_3N_4 coatings (upper layer), distance $75 \mu\text{m}$ from interface with Si_3N_4 -BN substrates (lower layer): compositions (a) 10 wt% BN, (b) 20 wt% BN, (c) 30 wt% BN. Indentations at $P = 100 \text{ N}$. Note how lower radial crack approaches and penetrates interface without delamination. Note also distortion of radial crack pattern at higher BN contents, indicating elastic-plastic mismatch.

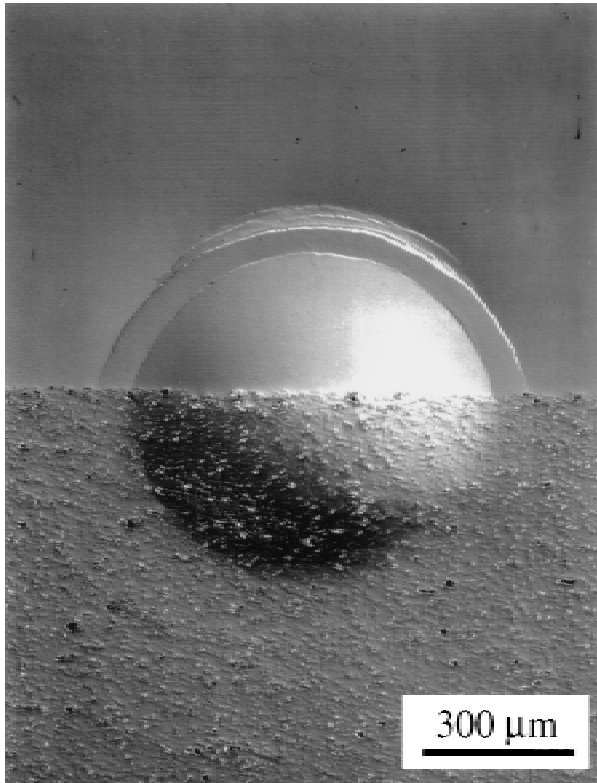


Fig. 2. Hertzian indentations in $\text{Si}_3\text{N}_4/\text{Si}_3\text{N}_4$ -10 wt% BN bilayer, made symmetrically across interface trace, with WC sphere $r = 1.98$ mm at $P = 2000$ N. Note crack penetration from Si_3N_4 side to Si_3N_4 -BN side, without delamination.

(3) Calibration of Indentation Stress–Strain Curves

Indentation stress–strain data for the individual component materials are plotted in Fig. 3. The solid curves in this figure are FEM-generated functions using measured values of Y , with E in the initial elastic region and α in the subsequent quasi-plastic region adjusted to give best fits (Table I). The monolithic silicon nitride shows slight nonlinearity in the stress–strain curve above the yield point at $p_Y = 1.1Y = 9.2$ GPa (Section II(2)).¹⁶ As the BN content increases, and Y and α simultaneously decrease (Table I), the curves deviate more from linearity, indicating the enhanced quasi-plasticity.⁷

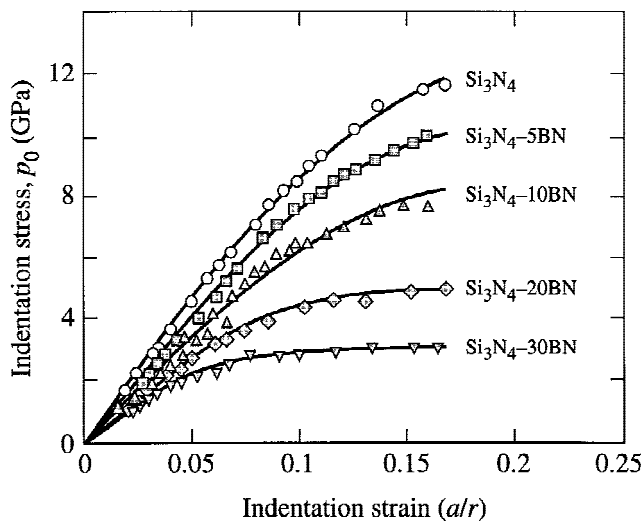


Fig. 3. Indentation stress–strain curves for component materials used in fabrication of $\text{Si}_3\text{N}_4/\text{Si}_3\text{N}_4$ -BN bilayers. Solid curves are FEM fits.

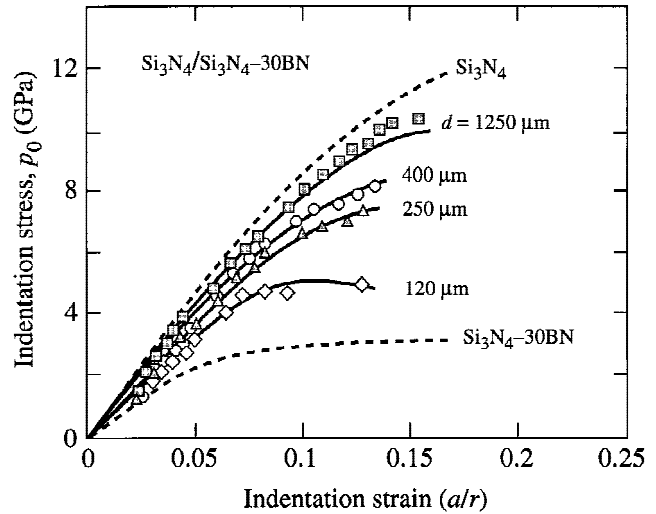


Fig. 4. Indentation stress–strain curves for $\text{Si}_3\text{N}_4/\text{Si}_3\text{N}_4$ -30 wt% BN bilayer composites, for Si_3N_4 coating thicknesses d indicated. Solid curves are FEM predictions, using material parameters calibrated from Fig. 3. Upper and lower dashed curves are bounds for Si_3N_4 and Si_3N_4 -30 wt% BN component materials, respectively, from Fig. 3.

Indentation stress–strain data for the $\text{Si}_3\text{N}_4/\text{Si}_3\text{N}_4$ -BN coating/substrate systems are shown in Figs. 4 and 5. In these figures the solid curves are now *a priori* FEM predictions, using the parameters calibrated from Fig. 3. Figure 4 shows curves for the different coating thicknesses, $d = 120, 250, 400,$ and 1250 μm , at fixed substrate composition 30 wt% BN. In this figure, the upper and lower dashed curves are bounds for monolithic Si_3N_4 and Si_3N_4 -30% BN respectively (from Fig. 3). The solid curves show a progressive shift away from the hard Si_3N_4 upper bound toward the soft Si_3N_4 -30% BN lower bound as the coating thickness decreases, indicating a correspondingly greater influence of the substrate material.⁴ (Note how this transition manifests itself as a maximum in the stress–strain curve in the $d = 120$ μm data, indicative of load transfer from coating to substrate.⁴) Figure 5 shows curves for the different substrate compositions, 10, 20, and 30 wt% BN, at fixed coating thickness $d = 250$ μm . Again, the upper dashed curve is the upper bound for monolithic Si_3N_4 . Once more, the

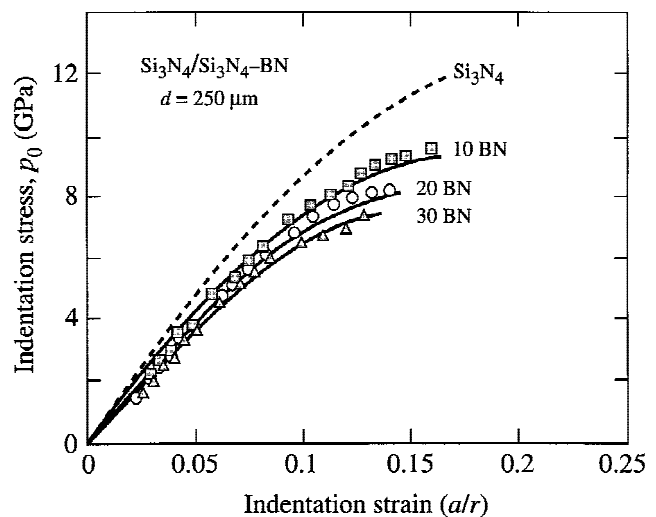


Fig. 5. Indentation stress–strain curves for $\text{Si}_3\text{N}_4/\text{Si}_3\text{N}_4$ -BN bilayer composites, Si_3N_4 coating thickness $d = 250$ μm , showing effect of BN content in substrate. Solid curves are FEM predictions, using material parameters calibrated from Fig. 3. Upper dashed curve is bound for Si_3N_4 from Fig. 3.

role of the soft substrate in determining the stress-bearing capacity of the composite bilayer is apparent.

IV. Results: Analysis of Transverse Fracture Patterns

We are now in a position to describe the fracture patterns observed in the silicon nitride bilayers, and to analyze the stress distributions responsible for this damage. In Figs. 6–9 we show section-view micrographs from bonded-interface specimens indented with a WC sphere of radius $r = 1.98$ mm, representing the effects of indentation load, substrate composition, and coating thickness. Corresponding FEM-generated contours of prin-

cipal stresses are included in Figs. 6, 8, and 9: principal shear stresses at left, shaded areas indicating yield zones ($\sigma_3 - \sigma_1 = Y$); principal normal stresses at right, shaded areas indicating tensile zones ($\sigma_1 \geq 0$), dashed curves indicating σ_3 stress trajectories (Fig. 6 only).

In this section we limit analysis of the stress fields to essentially qualitative aspects, deferring quantitative considerations to the Discussion.

(1) Effect of Indentation Load

Figure 6 shows a sequence of micrographs of Hertzian contact damage at increasing indentation load, $P = 800, 1000,$

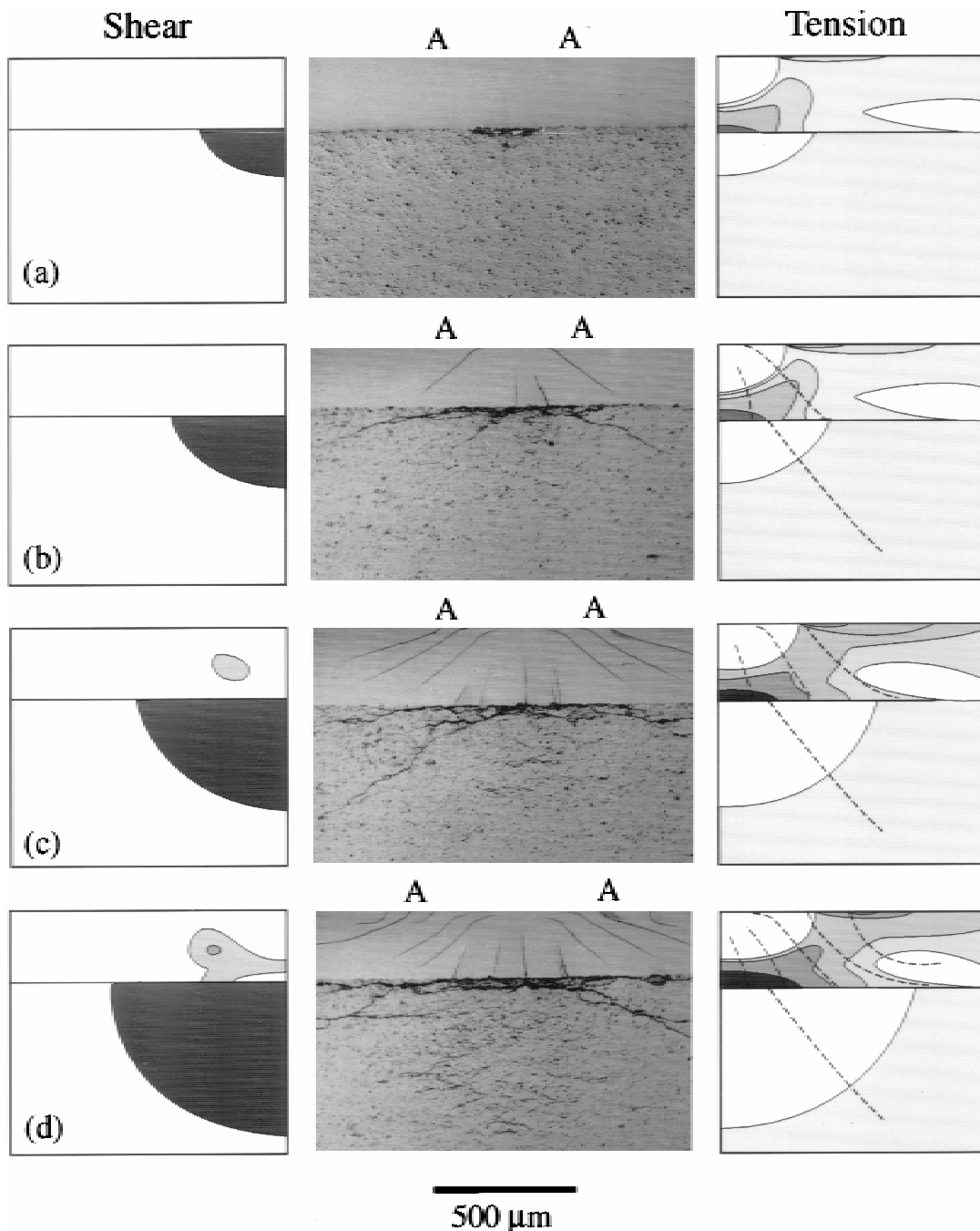


Fig. 6. Contact fracture in $\text{Si}_3\text{N}_4/\text{Si}_3\text{N}_4\text{-}30$ wt% BN bilayer composite, Si_3N_4 coating thickness $d = 250$ μm , using WC sphere $r = 1.98$ mm, illustrating the effect of indentation load: (a) $P = 800$ N, (b) $P = 1000$ N, (c) $P = 1500$ N, (d) $P = 2000$ N. Micrographs at center from bonded-interface specimens, Nomarski contrast. Arrows indicate contact diameter. Inner cracks initiate from coating/substrate interface, outer cracks from top surface, and intermediate cracks from within coating. Note the formation of a macroscopic quasi-plastic zone within the soft substrate at the higher loads. Corresponding FEM-generated contours of principal stresses included for comparison: left, principal shear stress, with shading indicating yield zones ($\sigma_3 - \sigma_1 = Y$); right, highest principal normal stress, shading indicating tensile zones ($\sigma_1 \geq 0$), dashed curves indicating σ_3 stress trajectories.

1500, and 2000 N, in $\text{Si}_3\text{N}_4/\text{Si}_3\text{N}_4$ -30 wt% BN fixed composition bilayers with coating thickness $d = 250 \mu\text{m}$. The most conspicuous damage in the hard Si_3N_4 coatings is a variety of transverse cracks, increasing in number with load: outer cracks initiating at the top surface outside the contact circle, extending downward and outward, in near-classical cone crack manner;¹⁶ inner cracks initiating from the coating/substrate interface closer to the inner contact axis, extending upward and inward;⁵ cracks initiating within the coating beneath the contact circle, intermediate in radial location between the prior two types in Fig. 6(d), extending upward and inward toward the top surface and downward and outward toward the lower interface. Serial sectioning by polishing away the top indented surface confirms that all of these cracks are essentially axisymmetrical, with consequent common (if distorted) quasi-conical geometry. For the coating/substrate configuration shown in Fig. 6, the first cracks to appear are those initiated at the interface ($P < 800 \text{ N}$), followed by those initiated within the coating ($P \approx 1000 \text{ N}$), and finally those initiated at the top surface ($P \approx 1200 \text{ N}$). A feature of the transverse cracks in Fig. 6 is that they appear to arrest as they approach the bounding surfaces of the coating, even through large load increases—the crack *density* is sensitive to load, crack *size* is not.

Substantial damage also occurs in the soft Si_3N_4 -30 wt% BN substrates in Fig. 6. There are indications of extensive quasi-plasticity in this sublayer.^{7,16} (Actually, limited quasi-plasticity is observed in the coatings as well, at higher magnification than in the micrographs in Fig. 6, especially at the higher loads.) Some accompanying cracking is also observed in the substrate, extending from the quasi-plastic damage zones and in some cases back to the interface. This combination of quasi-plasticity and cracking appears to contribute to minor interfacial delamination at the highest loads in Fig. 6. Control indentation tests on bulk Si_3N_4 -30 wt% BN specimens reveal only quasi-plastic damage, without any such accompanying cracking, indicating again that it is the layer configuration that enhances the fracture tendency.

The damage patterns in Fig. 6 may be compared with the FEM-generated shear and tensile stress fields at left and right. The intensity and spatial scale of these stress fields expand with the indentation load. In the coating, the locations of transverse crack initiation correlate strongly with the regions of high tensile stress concentration, indicated by degree of shading. A primary maximum in the tensile field occurs at the intersection of the coating/substrate interface with the contact axis; a secondary maximum occurs at the top surface outside the contact circle; and a saddle point occurs between these two maxima. Only the second of these concentrations is manifest in the classical Hertzian field in homogeneous solids,^{16,27} demonstrating again a significant influence of elastic-plastic mismatch on the stress distribution in the bilayer structure. The location of the surface maximum displaces increasingly beyond the contact circle with increasing load in Fig. 6, implying a progressive dilution of this maximum. Qualitatively, there also appears to be a correlation between the crack profiles and the FEM-generated stress trajectories²⁷ (although quantitatively, the trajectories are more steeply inclined to the top surface than the corresponding cracks by ≈ 5 – 10° , a discrepancy not atypical of Hertzian fractures²⁸). This correlation confirms that the fractures are predominantly mode I.

In the substrate, the locations of the quasi-plasticity zones correlate with the FEM-predicted yield boundaries in the shear contour plots in Fig. 6. (Note also that the shear stress contours indicate limited yield in the coating at the higher loads, consistent with the high-magnification observations referred to above.) The substrate yield zones become extensive at the higher loads; the implication is that the harder coating on its softer substrate support base sustains an ever-increasing component of “plate flexure” in its loading.⁴ The relatively minor cracking observed in the highly deformed anisotropic substrate layer does not appear to correlate quite as well with the tensile stress contour and trajectory patterns.

At higher loads, the damage intensifies and the system ultimately fails. An example is shown in Fig. 7 at $P \approx 4000 \text{ N}$, in a bilayer with 20 wt% BN substrate. In this case we show the half-surface as well as the side view. Excessive cracking is apparent. Comprehensive damage has occurred in the substrate, resulting in material removal and coating failure. The coating itself exhibits strong residual flexure from yield and multiple cracking.

(2) Effect of Substrate Composition

Figure 8 shows micrographs of Hertzian contact damage in $\text{Si}_3\text{N}_4/\text{Si}_3\text{N}_4$ -BN bilayers with 10, 20, and 30 wt% BN content in the substrate, for fixed coating thickness $d = 250 \mu\text{m}$ and load $P = 2000 \text{ N}$. In this sequence, the extent of transverse fracture in the coating and yield in the substrate increase markedly with BN content. Indeed, whereas the damage is well developed in the bilayer with 30 wt% BN substrate (Fig. 8(c), cf. Fig. 6(d)), the damage is only in its initiation stage in the bilayer with 10 wt% BN substrate (Fig. 8(a)). These results confirm most strongly the critical role of elastic-plastic mismatch in the damage mechanics. Again, the transverse fractures dominate delamination.

Comparison with the computed tensile and shear stress fields in Fig. 8 adds weight to the micrographic results. The intensity of both the coating tensile stress and substrate shear stress increases strongly with the elastic-plastic mismatch. Another manifestation of the mismatch is evident in the location of the primary maximum in the tensile field, at the top surface in the bilayer with 10 wt% BN substrate (as in the classical Hertzian field) but at the coating/substrate interface in the bilayer with 30 wt% BN substrate (cf. Fig. 11, later). Again, this implies an increasing component of plate flexure in the coating stress distribution with increasing mismatch. The yield boundaries in the shear field correlate with the sizes of the observed quasi-plasticity zones in the substrates.

(3) Effect of Coating Thickness

Figure 9 shows micrographs of Hertzian contact damage for diminishing Si_3N_4 coating thickness, $d = 1200, 400$ and 250

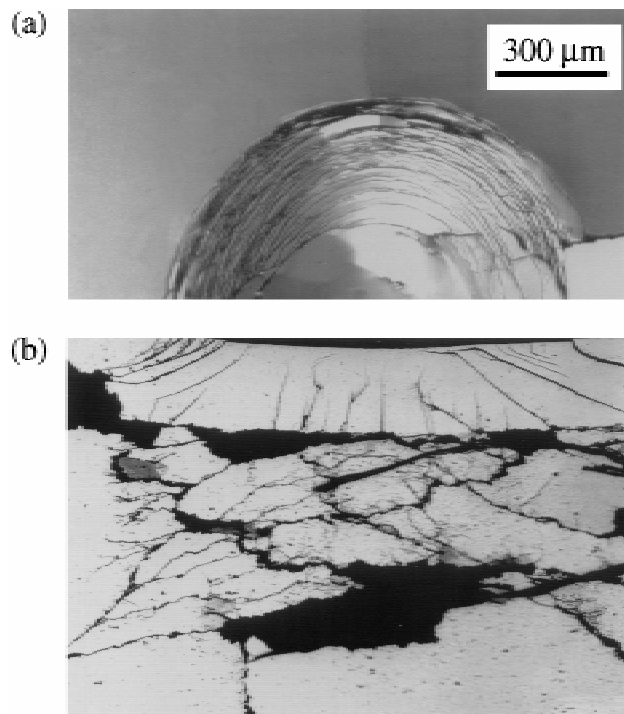


Fig. 7. Contact fracture in $\text{Si}_3\text{N}_4/\text{Si}_3\text{N}_4$ -20 wt% BN bilayer composite, Si_3N_4 coating thickness $d = 250 \mu\text{m}$, using WC sphere $r = 1.98 \text{ mm}$ at $P = 4000 \text{ N}$, showing half-surface (upper) and profile (lower) views. Note severe residual flexure of coating and coalescence of cracks leading to failure of coating and substrate.

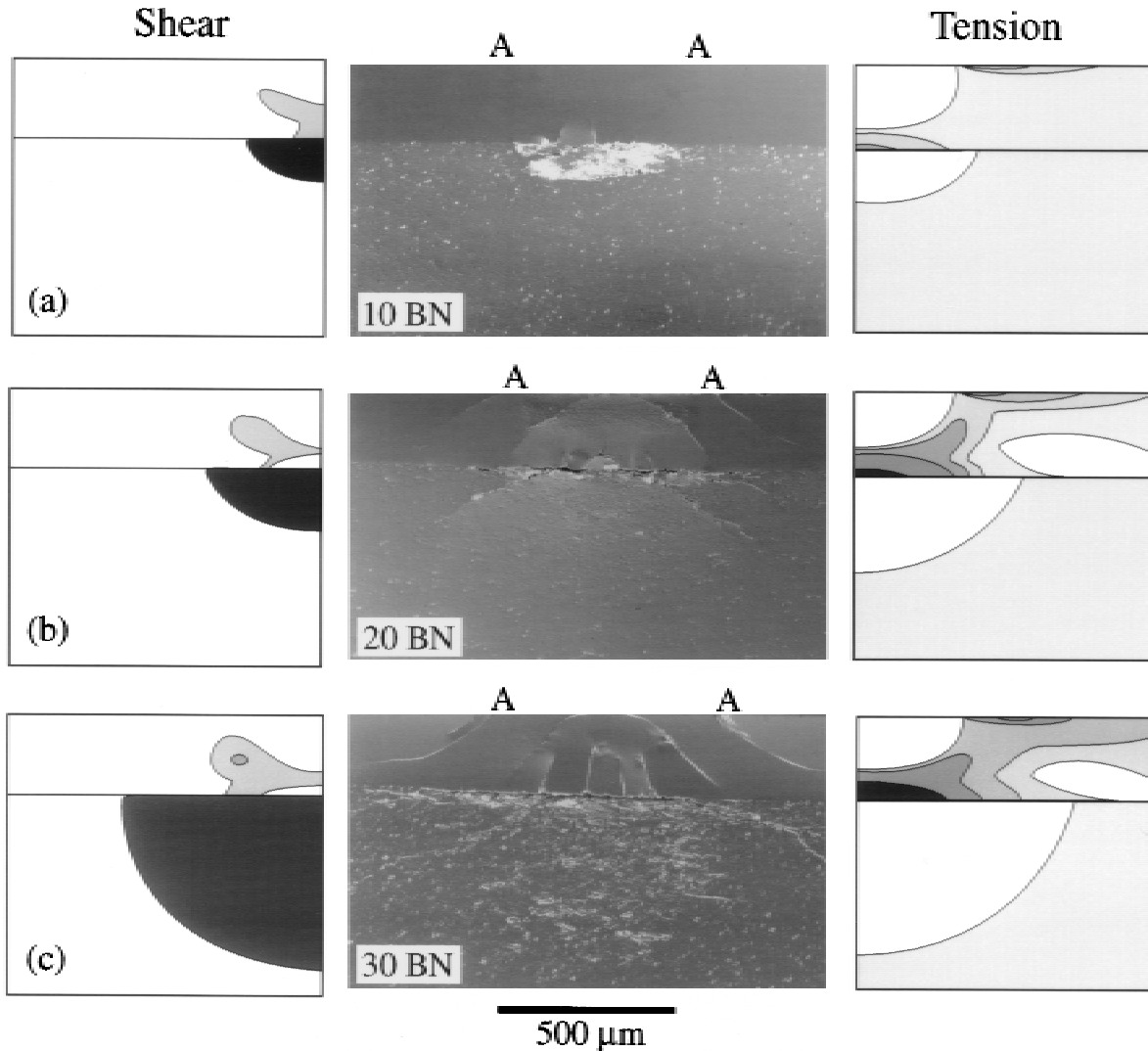


Fig. 8. Contact fracture in $\text{Si}_3\text{N}_4/\text{Si}_3\text{N}_4$ -BN bilayer composites, Si_3N_4 coating thickness $d = 250 \mu\text{m}$, using WC sphere $r = 1.98 \text{ mm}$ at $P = 2000 \text{ N}$, illustrating effect of substrate composition: (a) 10 wt% BN, (b) 20 wt% BN, (c) 30 wt% BN. Note increased damage at higher BN contents.

μm , in $\text{Si}_3\text{N}_4/\text{Si}_3\text{N}_4$ -30 wt% BN fixed composition bilayers at fixed load $P = 2000 \text{ N}$. No cracks are evident in the thickest coating (Fig. 9(a)): instead, the only damage is a limited subsurface quasi-plastic zone, akin to the damage seen in tougher monolithic Si_3N_4 materials.¹⁶ In the coating of intermediate thickness (Fig. 9(b)) the quasi-plastic damage is suppressed in favor of transverse fractures, in this case in their early stage of formation. On the other hand, some quasi-plasticity is now evident in the soft substrate. In the thinnest coating (Fig. 9(c)) the transverse crack pattern is well developed (cf. Fig. 6(d)), and yield in the substrate is substantial. The influence of layer geometry in promoting fracture in the coating is apparent.

Comparison with the computed stress fields accounts for the observed transition in mechanical response with coating thickness. The coating thickness in Fig. 9(a) is large compared with the contact zone, so the damage is little influenced by the presence of the substrate. In this case the stress fields are virtually indistinguishable from those of an ideal Hertzian contact: the maximum tensile stresses are concentrated at the outer top surface, and the maximum shear stresses directly below the contact area. In Fig. 9(b) the coating thickness and contact zone size are comparable, and the substrate begins to influence the damage pattern. The tensile stresses at the coating/substrate interface are now slightly greater than those at the top surface, as reflected in the appearance of interface as well as surface transverse cracks in the micrograph. Some yield is now evident

in the substrate. In Fig. 9(c) the coating thickness is smaller than the contact size, and the transverse crack pattern is well developed. The tensile stresses have intensified strongly at the coating/substrate interface. At the same time, the compression zones have also intensified, so the cracks, once initiated, are highly stabilized. This stabilization allows for the initiation of multiple transverse cracks. The yield zone in the substrate below the thin coating is now highly developed, implying once more an increased component of flexure in the overlying coating.

V. Discussion

In this study we have investigated the fracture behavior of silicon nitride bilayers with hard coatings of different thicknesses on softer substrates of different compositions. A feature of the bilayers is the presence of a relatively strong coating/substrate interface, where fracture energy is absorbed in the substrate rather than at the interface, with crack arrest rather than crack deflection.^{5,6,12,13} We have used Hertzian contacts on bonded-interface specimens to demonstrate the damage modes in these structures—transverse cracks in the coating, and quasi-plasticity in the substrate. The transverse cracks initiate at various locations in the coating: at the top surface, outside the contact circle (as in classical Hertzian fractures); within the interior of the coating, closer in below the contact

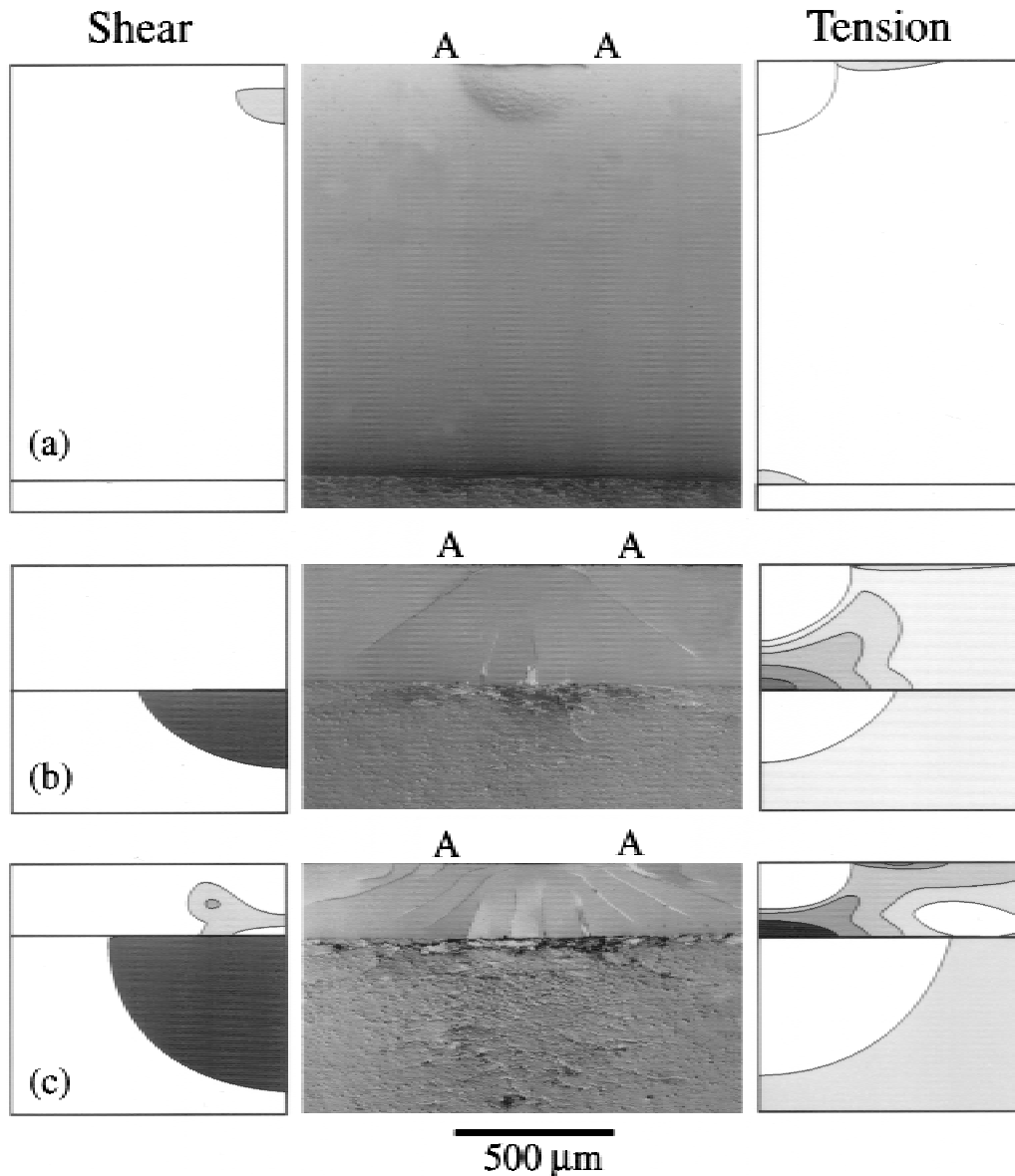


Fig. 9. Contact fracture in $\text{Si}_3\text{N}_4/\text{Si}_3\text{N}_4$ -30 wt% BN bilayer composites, Si_3N_4 , using WC sphere $r = 1.98$ mm at $P = 2000$ N, illustrating effect of coating thickness: (a) $d = 1200$ μm , (b) $d = 400$ μm , (c) $d = 250$ μm . Note increased damage at decreasing coating thickness.

circle; at the coating/substrate interface, immediately below the contact center. All three types are essentially axisymmetrical, with essentially quasi-conical geometry. There is a distinctive tendency away from surface-initiated toward interface-initiated fracture with increasing indenter load, decreasing coating thickness, and increasing elastic-plastic mismatch between layers.

The experimental observations in the bilayer structures are supported by FEM stress analysis, using calibrated elastic-plastic parameters from control tests on bulk constituent materials. For the coatings, we have demonstrated strong qualitative correlations between the calculated tensile stress extrema and the observed crack starting points, and between calculated stress trajectories and observed crack paths, implying predominantly mode I fracture. Some quantitative evaluations of the tensile stress maxima at the top surface and lower interface, for the same WC sphere radius $r = 1.98$ mm represented in Figs. 6–9, reinforce these correlations:

(i) *Effect of indentation load.* The solid curves in Fig. 10 are plots of the computed stress maxima as a function of load, for Si_3N_4 coating thickness $d = 250$ μm and Si_3N_4 -30 wt% BN substrate. The points on these curves correspond to the experimental loads $P = 800, 1000, 1500,$ and 2000 N in Fig.

6. Also indicated in Fig. 10 are the loads at which each kind of cracking initiates (C). Both maxima increase monotonically with load, the interface stress at a much faster rate than the surface stress. This is symptomatic of a highly nonlinear system (Fig. 4). Note that the interface maximum dominates the surface maximum above $P \approx 250$ N, explaining why the upward-extending interface cracks tend to form before the downward-extending surface cracks. The surface and interface stresses at the critical fracture loads in Fig. 10 are both significantly higher than the strengths of equivalent bulk Si_3N_4 monolith specimens (≈ 1000 MPa¹⁶), and are unequal, which is not atypical of crack systems in highly inhomogeneous stress fields.²⁹

(ii) *Effect of substrate composition.* In Fig. 11 we show the tensile stress maxima as a function of substrate BN composition, for $\text{Si}_3\text{N}_4/\text{Si}_3\text{N}_4$ -BN bilayers with Si_3N_4 coating thickness $d = 250$ μm at load $P = 2000$ N: again, the solid curves are the computed functions, and the data points correspond to the experimental BN contents 10, 20, and 30 wt% from Fig. 8. The interface stress maximum is sensitive to the BN content, but the surface stress maximum is not. This accounts for the increased density of upward-extending interface cracks for the 20% and 30% BN contents in Fig. 8. However,

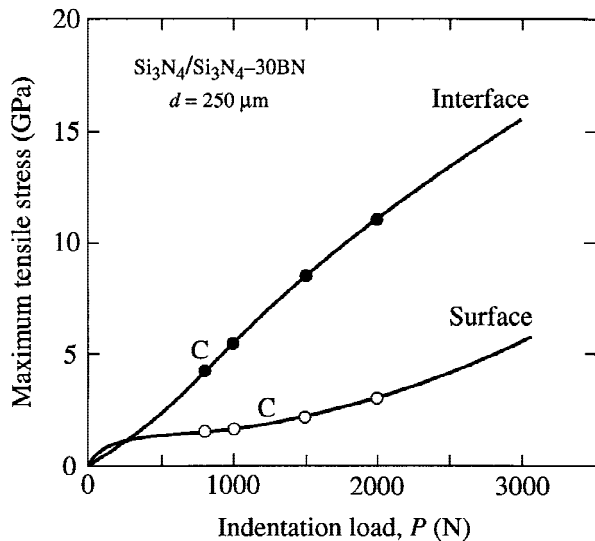


Fig. 10. Maximum principal tensile stresses in contact field in $\text{Si}_3\text{N}_4/\text{Si}_3\text{N}_4\text{-30 wt\% BN}$ bilayer composites as function of load, using WC sphere $r = 1.98$ mm. The two maxima shown occur at the top surface outside the contact and at the coating/substrate interface along the contact axis. Points C indicate onset of fracture. (Cf. Fig. 6.)

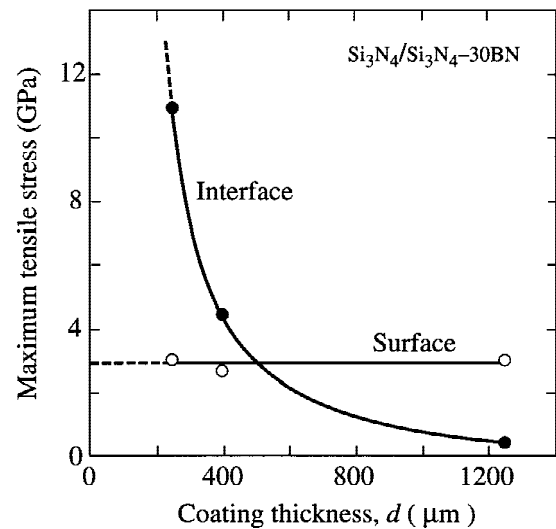


Fig. 12. Maximum principal tensile stresses in contact field in $\text{Si}_3\text{N}_4/\text{Si}_3\text{N}_4\text{-30 wt\% BN}$ bilayer composites as function of coating thickness, using WC sphere $r = 1.98$ mm at $P = 2000$ N. Dashed curves are extrapolations back to values at same locations in Si_3N_4 monolithic material. (Cf. Fig. 9.)

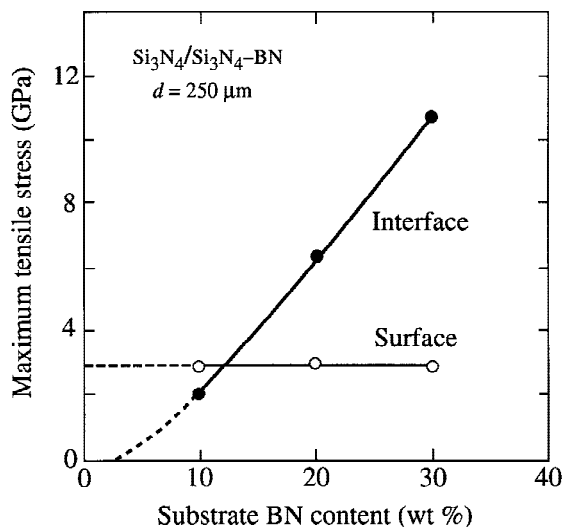


Fig. 11. Maximum principal tensile stresses in contact field in $\text{Si}_3\text{N}_4/\text{Si}_3\text{N}_4\text{-BN}$ bilayer composites with coating thickness $d = 250$ μm as function of BN composition in substrate, using WC sphere $r = 1.98$ mm at $P = 2000$ N. Dashed curves are extrapolations back to values at same locations in Si_3N_4 monolithic material. (Cf. Fig. 8.)

it does not account for the comparable increase in downward-extending surface cracks. It would appear that initiation of the first kind of cracks (interface) makes it easier to initiate the second (surface)—i.e., there are interaction effects. These observations highlight the influence of elastic-plastic mismatch.

(iii) *Effect of coating thickness.* In Fig. 12 we plot the tensile stress maxima as a function of Si_3N_4 coating thickness for $\text{Si}_3\text{N}_4/\text{Si}_3\text{N}_4\text{-30 wt\% BN}$ bilayers, at load $P = 2000$ N: the solid curves are the computed functions and the data points correspond to the experimental d values in Fig. 9. In similar fashion to Fig. 11, the interface stress maximum is sensitive to coating thickness, but the surface stress maximum is not. The interface maximum becomes increasingly dominant at smaller thicknesses. Accordingly, the density of upward-extending interface-initiated cracks, and subsequent accompanying interior-initiated and surface-initiated cracks, is considerably higher in the thinner coatings in Fig. 9.

These results indicate the changing nature of the coating tensile stress field from ideal “Hertzian” to effectively “flexural” with increasing load, decreasing substrate hardness relative to the coating (mismatch), and decreasing coating thickness. At high loads hard, thin coatings on thick, soft substrates deform more as flexing plates with supported outer edges (where the encasing substrate remains elastic), shifting the tensile stress concentration progressively away from the upper outer free surface through the coating interior toward the lower coating/substrate interface.^{3,4,7,21,22} At the same time, the flexure induces highly compressive stresses on the opposing sides of the neutral planes within the coating. The result is the arrays of highly stabilized transverse coating fractures seen in Figs. 6–10.

The quantitative analysis of the crack systems described here is by no means complete. The FEM algorithm enables one to investigate prescribed indentation and coating variables (load, mismatch, coating thickness) numerically. The complexity of the highly nonlinear and inhomogeneous tensile stress fields would appear to preclude analytical fracture mechanics solutions. Moreover, even the elastic-plastic FEM solutions described in Sections III and IV are restrictive. They pertain strictly to uncracked bodies, whereas the coatings considered here contain multiple cracks. The capacity of fracture mechanics to determining ensuing crack energies and paths from pre-existing (precrack) contact fields in finite bodies with an acceptable degree of accuracy has been shown to be limited, even for single cone fractures in monolithic, homogeneous elastic bodies.²⁸ Such limitations are likely to be even more apparent in the multiple crack systems in the layered, inhomogeneous inelastic bodies of interest here. More objective numerical procedures that enable piecewise determinations of crack growth in the ever-evolving rather than the prior stress field would appear to be necessary for the determination of appropriate mechanical-energy-release rates or stress-intensity factors.²⁸ This is especially the case in determining crack evolution histories, and in seeking accounts of the enhanced crack stability and multiplicity in thinner coatings on softer substrates.

There are other potential complications that we have minimized in this study. First, macroscopic in-plane layer residual stresses from thermal expansion mismatch or sintering stresses can also have a strong influence on the crack behavior, leading to suppression of coating fracture in favorable circumstances.^{12,13} In our bilayer systems such in-plane stresses ap-

pear to be negligibly small (Section III(2)). Second, local residual tensile stresses around indentation quasi-plasticity zones are known to have profound effects on crack evolution during unloading,^{30,31} especially in layer structures with yielding substrates; whereas residual stresses do not appear to have much influence on the transverse cracks, they can be especially effective in opening up any interfacial delamination cracks during the unloading half-cycle.⁴ The observation that delamination is minimal in our silicon nitride bilayer systems provides some justification for ignoring unloading effects in our FEM calculations. Finally, anisotropy is another factor that can exert a strong influence on fracture behavior. The highly textured microstructures in the Si₃N₄-BN bilayers may explain the tendency for substrate cracks to align themselves parallel to the interface in Figs. 6–9.

The crack patterns identified in this study are of interest in relation to engineering layer design. Transverse cracks may be expected to play a major role in the failure of ceramic coating structures where contact stress concentrations are a common form of loading, e.g., in bearings, cutting tools, surface-coated engine components, and so on. This class of cracks is particularly relevant to layer structures with strongly bonded coating/substrate interfaces. In this context, the transverse cracks are highly stable, leading to multiple initiation with consequent energy absorption, so that even highly brittle coating systems can be damage tolerant. (Again, superposed compression stresses could help reduce or even suppress transverse coating fracture.) This high stability means that the crack sizes are governed more by the layer thickness than by material properties; the cracks tend to contain themselves within the boundaries of the coating over a wide range of contact loads. On the other hand, initiation of the cracks will surely be sensitive to material properties, such as elastic-plastic mismatch (e.g., Fig. 8) and coating toughness. For optimum substrate protection the present results indicate hard, tough coatings with low elastic-plastic mismatch, with thicknesses at least as large as the characteristic contact dimensions. As always, these requirements must ultimately be balanced against the costs of fabrication and finishing.

Acknowledgments: K. S. Lee and S. Wuttiphphan wish to thank Do Kyung Kim at the Korea Advanced Institute of Science and Technology and Isabel K. Lloyd at the University of Maryland for their encouragement and support. Ralph F. Krause assisted with the hot pressing of the silicon nitride structures. Anthony C. Fischer-Cripps set up the original finite element algorithm used in this study. Shi-Woo Lee and Jae-Hun Kim assisted with the plasma etching and SEM analysis.

References

- ¹J. C. Knight, T. F. Page, and I. M. Hutchings, "The Influence of Substrate Hardness on the Response of TiN-Coated Steels to Surface Deformation," *Thin Solid Films*, **177**, 117–32 (1989).
- ²M. V. Swain and J. Mencik, "Mechanical Property Characterization of Thin Films Using Spherical Tipped Indenters," *Thin Solid Films*, **253**, 204–11 (1994).
- ³A. Pajares, L. Wei, B. R. Lawn, N. P. Padture, and C. C. Berndt, "Mechanical Characterization of Plasma-Sprayed Ceramic Coatings on Metal Substrates by Contact Testing," *Mater. Sci. Eng.*, **A208** [2] 158–65 (1996).
- ⁴A. Pajares, L. Wei, B. R. Lawn, and C. C. Berndt, "Contact Damage in Plasma-Sprayed Alumina-Based Coatings," *J. Am. Ceram. Soc.*, **79** [7] 1907–14 (1996).
- ⁵L. An, H. M. Chan, N. P. Padture, and B. R. Lawn, "Damage-Resistant Alumina-Based Layer Composites," *J. Mater. Res.*, **11** [1] 204–10 (1996).
- ⁶S. Wuttiphphan, B. R. Lawn, and N. P. Padture, "Crack Suppression in Strongly-Bonded Homogeneous/Heterogeneous Laminates: A Study on Glass/Glass-Ceramic Bilayers," *J. Am. Ceram. Soc.*, **79** [3] 634–40 (1996).
- ⁷H. Liu, B. R. Lawn, and S. M. Hsu, "Hertzian Contact Response of Tailored Silicon Nitride Multilayers," *J. Am. Ceram. Soc.*, **79** [4] 1009–14 (1996).
- ⁸A. G. Evans and J. W. Hutchinson, "On the Mechanics of Delamination and Spalling in Compressed Films," *Int. J. Solids Struct.*, **20** [5] 455–66 (1984).
- ⁹J. B. Davis, H. C. Cao, G. Bao, and A. G. Evans, "The Fracture Energy of Interfaces: An Elastic Indentation Technique," *Acta Metall.*, **39** [5] 1019–24 (1991).
- ¹⁰J. W. Hutchinson and Z. Suo, "Mixed-Mode Cracking in Layered Structures," *Adv. Appl. Mech.*, **29**, 64 (1991).
- ¹¹W. J. Clegg, K. Kendall, N. M. Alford, T. W. Button, and J. D. Birchall, "A Simple Way to Make Tough Ceramics," *Nature (London)*, **347**, 455–57 (1991).
- ¹²O. Prakash, P. Sarkar, and P. S. Nicholson, "Crack Deflection in Ceramic/Ceramic Laminates with Strong Interfaces," *J. Am. Ceram. Soc.*, **78** [4] 1125–27 (1995).
- ¹³H. M. Chan, "Layered Ceramics: Processing and Mechanical Behavior," *Annu. Rev. Mater. Sci.*, **27**, 249–82 (1997).
- ¹⁴H. Liu and S. M. Hsu, "Fracture Behavior of Multilayer Silicon Nitride/Boron Nitride Ceramics," *J. Am. Ceram. Soc.*, **79** [9] 2452–57 (1996).
- ¹⁵B. R. Lawn, N. P. Padture, H. Cai, and F. Guiberteau, "Making Ceramics 'Ductile,'" *Science*, **263**, 1114–16 (1994).
- ¹⁶S. K. Lee, S. Wuttiphphan, and B. R. Lawn, "Role of Microstructure in Hertzian Contact Damage in Silicon Nitride: I, Mechanical Characterization," *J. Am. Ceram. Soc.*, **80** [9] 2367–81 (1997).
- ¹⁷H. Cai, M. A. Stevens Kalceff, and B. R. Lawn, "Deformation and Fracture of Mica-Containing Glass-Ceramics in Hertzian Contacts," *J. Mater. Res.*, **9** [3] 762–70 (1994).
- ¹⁸F. Guiberteau, N. P. Padture, H. Cai, and B. R. Lawn, "Indentation Fatigue: A Simple Cyclic Hertzian Test for Measuring Damage Accumulation in Polycrystalline Ceramics," *Philos. Mag. A*, **68** [5] 1003–16 (1993).
- ¹⁹D. Tabor, *Hardness of Metals*. Clarendon, Oxford, U.K., 1951.
- ²⁰A. C. Fischer-Cripps and B. R. Lawn, "Indentation Stress-Strain Curves for 'Quasi-Ductile' Ceramics," *Acta Metall.*, **44** [2] 519–27 (1996).
- ²¹A. C. Fischer-Cripps, B. R. Lawn, A. Pajares, and L. Wei, "Stress Analysis of Elastic-Plastic Contact Damage in Ceramic Coatings on Metal Substrates," *J. Am. Ceram. Soc.*, **79** [10] 2619–25 (1996).
- ²²S. Wuttiphphan, A. Pajares, B. R. Lawn, and C. C. Berndt, "Effect of Substrate and Bond Coat on Contact Damage in Zirconia-Based Plasma Coatings," *Thin Solid Films*, **293** [1–2] 251–60 (1997).
- ²³K. Komvopoulou, "Elastic-Plastic Finite Element Analysis of Indented Layered Media," *J. Tribol.*, **111**, 430–39 (1989).
- ²⁴P. Montmitonnet, M. L. Edinger, and E. Felder, "Finite Element Analysis of Elastoplastic Indentation: Part II—Application to Hard Coatings," *J. Tribol.*, **115**, 15–19 (1993).
- ²⁵M.-W. He and J. W. Hutchinson, "Crack Deflection at an Interface Between Dissimilar Elastic Materials," *Int. J. Solids Struct.*, **25** [9] 1053–67 (1989).
- ²⁶T. J. Lardner, J. E. Ritter, M. L. Shiao, and M. R. Lin, "Behavior of Indentation Cracks Near Free Surfaces and Interfaces," *Int. J. Fract.*, **44**, 133–43 (1990).
- ²⁷F. C. Frank and B. R. Lawn, "On the Theory of Hertzian Fracture," *Proc. R. Soc. London*, **A299** [1458] 291–306 (1967).
- ²⁸C. Kocer and R. E. Collins, "The Angle of Hertzian Cone Cracks," *J. Am. Ceram. Soc.*, in press.
- ²⁹B. R. Lawn and T. R. Wilshaw, "Indentation Fracture: Principles and Applications," *J. Mater. Sci.*, **10** [6] 1049–81 (1975).
- ³⁰D. B. Marshall and B. R. Lawn, "Residual Stress Effects in Sharp-Contact Cracking: I. Indentation Fracture Mechanics," *J. Mater. Sci.*, **14** [8] 2001–12 (1979).
- ³¹B. R. Lawn, A. G. Evans, and D. B. Marshall, "Elastic/Plastic Indentation Damage in Ceramics: The Median/Radial Crack System," *J. Am. Ceram. Soc.*, **63** [9–10] 574–81 (1980). □